Oxidation of $TaSi_2$-Containing ZrB_2-SiC Ultra-High Temperature Materials

Elizabeth J. Opila[*,1], Jim Smith, Stanley R. Levine[1,2], Jonathan Lorincz[3] and Marissa Reigel[4]

[1]*NASA Glenn Research Center, Cleveland, Ohio, OH 44135, USA*

[2]*Retired*

[3]*CONTECH Construction Products Inc., Englewood, CO 80111, USA*

[4]*Savannah River Nuclear Solutions, Aiken, SC 29803, USA*

Abstract: Hot pressed coupons of composition ZrB_2 -20 v% SiC -5 v% $TaSi_2$ and ZrB_2 -20 v% SiC -20 v% $TaSi_2$ were oxidized in stagnant air at temperatures of 1627 and 1927°C for one, five and ten 10-minute cycles. The oxidation reactions were characterized by weight change kinetics, x-ray diffraction, and SEM/EDS. Detailed WDS/microprobe quantitative analyses of the oxidation products were conducted for the ZrB_2 -20 v% SiC -20 v% $TaSi_2$ sample oxidized for five 10-minute cycles at 1927°C. Oxidation kinetics and product formation were compared to ZrB_2 -20 v% SiC with no $TaSi_2$ additions. It was found that the 20 v% $TaSi_2$ composition exhibited improved oxidation resistance relative to the material with no $TaSi_2$ additions at 1627°C. However, for exposures at 1927°C less oxidation resistance and extensive liquid phase formation were observed compared to the material with no $TaSi_2$ additions. Attempts to limit the liquid phase formation by reducing the $TaSi_2$ content to 5 v% were unsuccessful. In addition, the enhanced oxidation resistance at 1627°C due to 20 v% $TaSi_2$ additions was not achieved at the 5 v% addition level. The observed oxidation product evolution is discussed in terms of thermodynamics and phase equilibria for the $TaSi_2$-containing ZrB_2-SiC material system. $TaSi_2$-additions to ZrB_2-SiC at any level are not recommended for ultra-high temperature (>1900°C) applications due to excessive liquid phase formation.

Keywords: ZrB_2, SiC, $TaSi_2$, Oxidation kinetics, Furnace testing, Microstructural characterization.

INTRODUCTION

ZrB_2 and related materials are considered for ultra-high temperature applications such as leading edges of hypersonic vehicles due to their high melting points. However, application of these materials is limited due to their poor oxidation resistance, low toughness, and low thermal shock resistance [1]. This paper addresses methods to improve the oxidation resistance of ZrB_2. ZrB_2 oxidizes to form B_2O_3 and ZrO_2. At temperatures between 450 and about 1100°C, liquid phase boria is formed [2]. This liquid phase provides a somewhat protective liquid layer that slows oxygen transport to the underlying substrate. At temperatures greater than 1100°C, the B_2O_3 boils off allowing rapid transport of oxygen through the zirconia scale to the underlying ZrB_2 substrate. Additions of 20 v% SiC to ZrB_2 [3] provided improved oxidation resistance since the formation of a silica scale provides protection to much higher temperatures dependent on the amount of additive and oxidation condition [4]. However, at temperatures above the melting point of silica (T_m=1723°C [5]), the liquid film can be lost to volatility and shear forces in high velocity applications [6]. Many studies have been conducted to add additional constituents to the ZrB_2-SiC system in attempts to further increase the oxidation resistance. $TaSi_2$ is one such constituent that has been considered to increase the oxidation resistance.

*Address correspondence to this author at the NASA Glenn Research Center, Cleveland, Ohio, OH 44135, USA; Tel: 001 216-433-8904; Fax: 001 216-433-5544; E-mail: opila@nasa.gov

It has been demonstrated that Ta additions to ZrB_2-based materials showed improved oxidation resistance relative to the baseline materials at moderately high temperatures (T≤1627°C). Talmy *et al.* showed that two to twenty mol% TaB_2 additions to ZrB_2-SiC resulted in improved oxidation resistance at temperatures between 1200 and 1400°C [7]. Similarly, Ta_5Si_3 and $TaSi_2$ additions in the amounts of 8-31 v% showed improved oxidation resistance relative to ZrB_2 at temperatures between 1100 and 1400°C in air for times of two to three hours [8,9]. In all cases, Talmy showed evidence for immiscible glass formation in the oxidation products and attributed the improved oxidation resistance to the steeply rising liquidus temperatures, increased viscosity, and decreased oxygen diffusivity [7] of the phase-separated glasses. Opila *et al.* [10] showed that ZrB_2 - 20 v% SiC -20 v% $TaSi_2$ resulted in a ten-fold reduction in oxide thickness relative to ZrB_2 -20 v% SiC after oxidation at 1627°C for 100 minutes in stagnant air. This improvement was attributed to the presence of Ta rather than the increased Si-content. The mechanism for improved oxidation behavior was not determined, however, it was proposed that this result was either due to formation of immiscible glass phases or Ta-doping of the ZrO_2 scale.

$TaSi_2$ has a melting point of approximately 2200°C [11,12] so the material itself has high temperature capability. The expected oxidation products, SiO_2 and Ta_2O_5 have melting points of 1723°C [5] and 1872°C (α-Ta_2O_5) [13] respectively. Upon oxidation at temperatures above 1872°C,

1874-1460/10

$TaSi_2$ is therefore expected to form a liquid phase. For mixed ZrB_2-SiC-$TaSi_2$, the oxidation products are expected to be more complex. The formation of Ta_2O_5-xZrO_2 phase V with x reportedly varying between 5 and 8 [14-16] is possible. The melting temperature of this phase is unknown, but has been reported to be >1870°C [14]. Thus, this oxidation product is also likely to limit the temperature capability of $TaSi_2$-containing ZrB_2-SiC compositions. It was proposed [10] that additions of small amounts (<20v%) of $TaSi_2$ to ZrB_2 might result in oxidation to form Ta_2O_5 in solution with ZrO_2, thus preventing formation of these low melting oxides. While the extent of Ta_2O_5 solubility is unknown, a phase diagram for the related Nb_2O_5-ZrO_2 system shows 5 to 10 mol% solubility of Nb_2O_5 in ZrO_2 [16].

The objectives of this work are to: 1) Extend the previous work with ZrB_2 -20 v% SiC -20 v% $TaSi_2$ [10] to the lower $TaSi_2$ level of 5 v% for developing enhanced oxidation resistance at both 1627 and 1927°C, and 2) Interpret the results of a detailed characterization of ZrB_2 -20 v% SiC -20 v% $TaSi_2$ before and after oxidation using microprobe and quantitative WDS to understand liquid phase formation arising from $TaSi_2$ additions, the whereabouts of the Ta in the oxide scale, and possible steps to mitigate liquid-phase formation.

MATERIALS AND METHODOLOGY

ZrB_2-SiC-$TaSi_2$ coupons were prepared from powders described in Table **1**. Processing history is summarized in Table **2**. Several batches of the same composition were made. The powders were mixed, and then milled using Si_3N_4 media in hexane in a Si_3N_4 mill for 24 h. The powders were vacuum hot pressed using a graphite die. Further details can be found in reference [17]. Sample coupons of 2.5 cm × 1.2 cm × 0.3 cm were machined from hot pressed plates. The coupons were ultrasonically cleaned in detergent (Micro-90, International Products Corporation), de-ionized water, acetone, and alcohol prior to oxidation. X-ray diffraction and Energy Dispersive Spectroscopy of as-machined and cleaned coupons indicated ZS20TS contained ZrB_2, SiC, $TaSi_2$ and a minor amount of a (Zr,Ta) boride solution.

Table 1. Powders Used for Sample Preparation

Material	Source	Particle Size	Purity%
ZrB_2	Cerac	<10μm	99.5
SiC	HC Starck	<5 μm	>99.9
$TaSi_2$	Cerac	80% -325 mesh (-44 μm)	>99.9

Initial surface areas and sample weights were recorded. The samples were oxidized at 1627°C in stagnant air in a bottom loading CM Inc. $MoSi_2$ element box furnace. The samples were oxidized at 1927°C in stagnant air in a bottom loading DelTech, Inc. zirconia element furnace. Three coupons were loaded into a slotted calcia-stabilized zirconia firebrick setter (98.7% purity). Two lines of contact existed between the setter and sample. The coupons were oxidized for ten minute cycles. On heat-up to 1627°C, the furnace temperature reached approximately 100 degrees less than the set temperature in 1 minute. Heating to the set temperature was complete 5 minutes into the heating cycle. The DelTech furnace temperature fell by approximately 75 degrees during the loading process. Samples were removed from the furnace and cooled in ambient conditions for 10 minutes between cycles. A coupon was removed after one cycle, five cycles, and ten cycles. A maximum oxidation time of 100 minutes was achieved. Post-oxidation weight changes were recorded where possible. Some coupons stuck to the zirconia setter due to extensive glass formation.

Optical macrographs were taken of all coupons after oxidation. The sample surfaces were analyzed by X-Ray Diffraction (XRD), Field Emission Scanning Electron Microscopy (FESEM) Hitachi S-4700, and Energy Dispersive Spectroscopy (EDS) to determine phases present before and after oxidation as well as oxide microstructures. Several materials were also examined by FESEM and EDS in cross-section prepared by non-aqueous cutting and polishing procedures to preserve boria-containing phases. The ZSTS20 coupon previously oxidized for five cycles (50 minutes total exposure) at 1927°C was also characterized extensively by Wavelength Dispersive Spectroscopy (WDS) microprobe (JEOL 8200). Each reported phase composition determined by microprobe is the average of five measurements.

RESULTS

Oxidation Kinetics

The weight change results for ZS, ZSTS5, and ZSTS20 obtained at 1627°C in stagnant air are shown in Fig. (**1**). Macrophotos of the materials after oxidation at 1627°C are shown in Fig. (**2**). Surface SEM images are shown in Fig. (**3**) for all three compositions while cross sections of the oxide scale are shown in Fig. (**4**). XRD results for all the oxidized materials were similar and showed only ZrO_2 (monoclinic) with minor amounts of ZrO_2 (cubic). No additional phases were observed. Macrographs of ZS, ZSTS5, and ZSTS20

Table 2. Summary of Compositions, Designations, and Processing

Composition	Designation/Oxidation Temperature (°C)	Processing	Density, g/cm^3	Relative Density, %
ZrB_2-20 v% SiC	ZS	2000°C, 10ksi, 2h	5.27	95.5
ZrB_2 -20 v% SiC -20 v% $TaSi_2$	ZSTS20-1627	1600°C, 10ksi, 2h	5.92	97.7
ZrB_2 -20 v% SiC -20 v% $TaSi_2$	ZSTS20-1927	1600°C, 10ksi, 2h	6.04	99.7
ZrB_2 -20 v% SiC -5 v% $TaSi_2$	ZSTS5-1627	1750°C, 10ksi, 2h	5.52	97.6
ZrB_2 -20 v% SiC -5 v% $TaSi_2$	ZSTS5-1927	1700°C, 10ksi, 2h	5.45	96.3

after oxidation at 1927°C are shown in Fig. (**5**). The results for ZS and ZSTS20 were previously published [10] but are shown here for comparison.

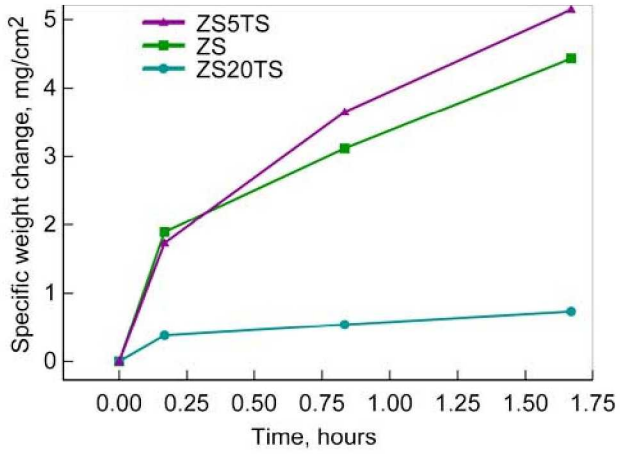

Fig. (1). Weight change results obtained at 1627°C in stagnant air for ZrB_2-20 v% SiC baseline material compared to compositions containing 5 and 20 v% $TaSi_2$. ZS and ZS20TS from ref. [9].

The weight change results and macrophotos for the sample exposed at 1627°C show that ZrB_2 -20 v% SiC -20 v% $TaSi_2$ shows the best oxidation behavior. The addition of 5 v% $TaSi_2$ to ZrB_2 -20 v% SiC is insufficient to lead to phase separation in the glass, whereas 20 v% $TaSi_2$ additions result in immiscible glass formation as shown in Fig. (**3**). The oxidation thickness is reduced approximately ten times for 20 v% $TaSi_2$ relative to the material with no additives as shown in Fig. (**4**) [10]. The oxide cross-section for the sample with 5 v% $TaSi_2$ is not shown since the scale was bubbled and varied irregularly in thickness between 4 and 100 μm for a sampling of 20 locations. At 1927°C, the material with no $TaSi_2$ exhibits the best oxidation behavior since liquid phase formation is limited. Extensive liquid formation is observed for both the 5 and 20 v% $TaSi_2$ addition levels.

Microstructural/Compositional Characterization of ZSTS20 Before and After 1927°C Exposure in Stagnant Air for 50 Minutes

In previous work [10], EDS analysis of the ZSTS oxidation products was complicated by the fact that the Ta Mα peak (1.709 keV) has almost complete overlap with the Si Kα peak (1.739 keV). Ta identification was made primarily by observing the low intensity Ta Lα peak at 8.145 keV. In addition, phases with high Si content had much darker contrast than those with high Ta content. Nevertheless, it was uncertain where Ta was incorporated into the oxidation products. In addition, the composition of the low melting phase was unknown, preventing an understanding of possible ways to improve the high temperature oxidation resistance of ZSTS materials. In this paper, microprobe wavelength dispersive spectroscopy (WDS) was used to more completely characterize the oxidation products. The following microprobe results are presented beginning with the substrate and proceeding outward through the layers of the oxide products formed to identify the key reactions occurring during the oxidation exposure at 1927°C. Results are summarized in Table **3**.

Substrate Before Oxidation

After hot pressing, in addition to the starting phases ZrB_2, SiC, and $TaSi_2$, an additional phase zirconium rich boride phase $(Zr,Ta)B_x$ was observed as shown in Fig. (**6**). This solution phase has been previously observed [8,10] and is reasonable since both ZrB_2 and TaB_2 have a hexagonal crystal structure. XRD results showed that the (100), (101), and (111) peaks for ZrB_2 all exhibited shoulders displaced by 0.1 to 0.5 degrees 2theta higher indicating reduction of the lattice parameters of the hexagonal ZrB_2 structure with the introduction of TaB_2

Substrate After Oxidation

After oxidation, the $TaSi_2$ is no longer found in the substrate throughout the entire thickness as shown in Fig. (**6**). Fig. (**6b**) was obtained near the center of the coupon. The Ta is now present as a carbide $(Ta,Zr)C_x$. The amount of ZrB_2 and SiC have both decreased relative to the starting material whereas the amount of $(Zr,Ta)B_x$ phase has increased. Porosity is found throughout the substrate.

Substrate Near Oxide Interface

Fig. (**7**) shows elemental analysis at the substrate/oxide interface. Note that ZrB_2 and SiO_2 are present just below ZrO_2-containing oxide scale in a very thin layer. Below this layer, all Si-containing phases are depleted for approximately 150 μm.

Oxide Near Oxide Interface

Figs. (**7**, **8**) show that Ta is found near the ZrB_2/ZrO_2 interface in the small (~1 μm) grains of Ta oxyborides with brightest contrast. Large ZrO_2 grains are observed in a sea of SiO_2. Figs. (**7**, **8**) also show that Ta and B are present at low levels throughout much of the oxide scale.

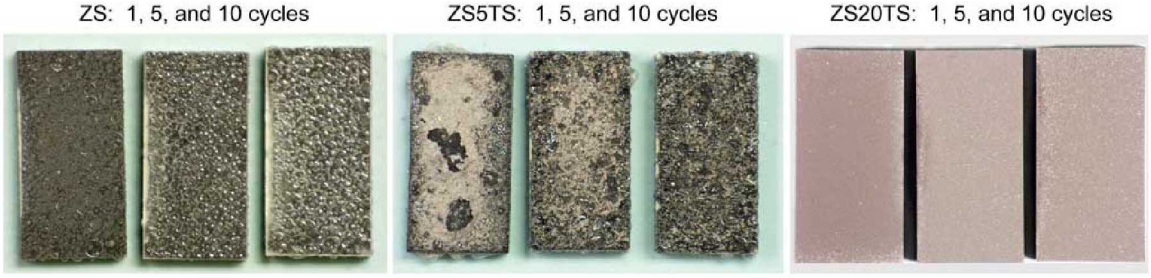

Fig. (2). Macrophotos of coupons after oxidation at 1627°C in stagnant air.

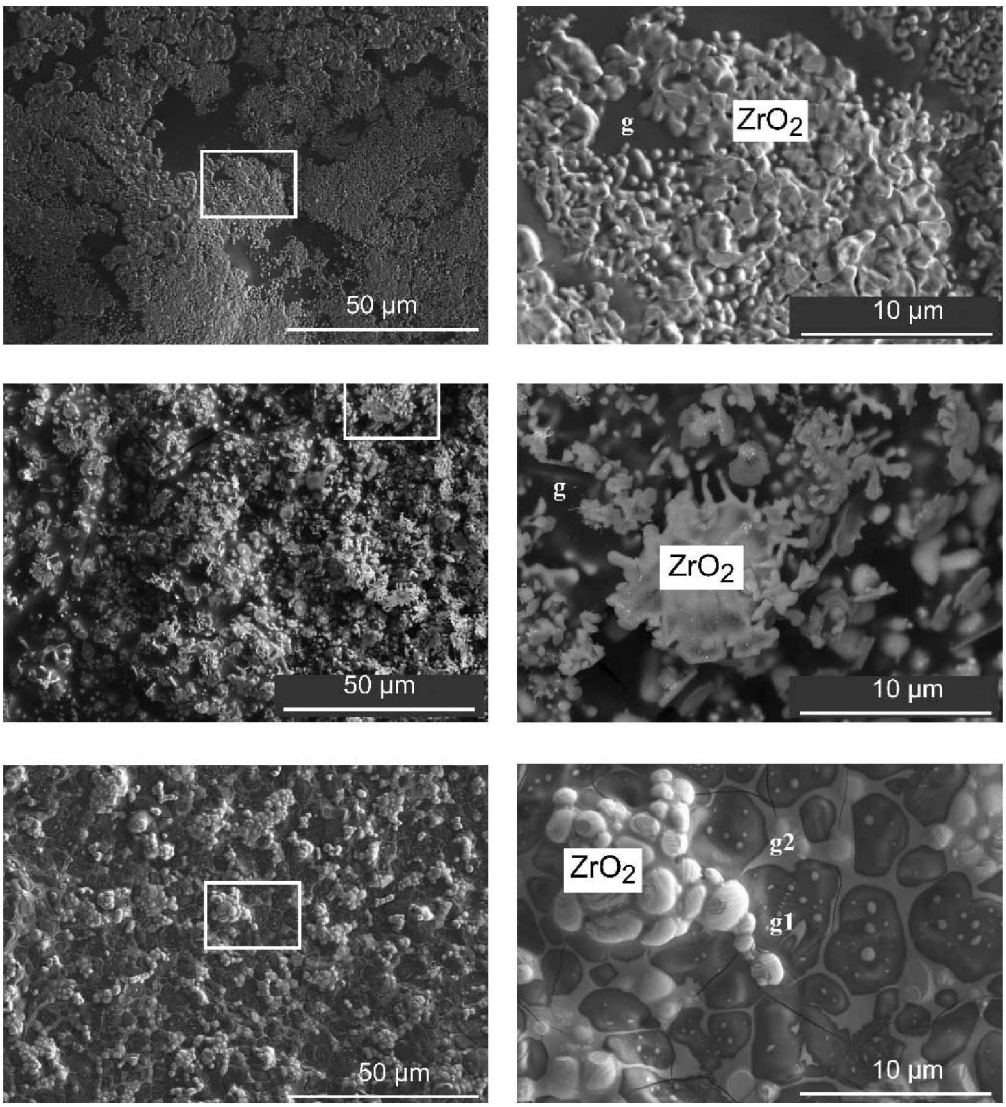

Fig. (3). Secondary electron images showing surface morphology of the ZS (top), ZSTS5 (middle), and ZSTS20 (bottom) after oxidation at 1627°C for 100 min in stagnant air. Details of area in white box on left are shown in higher magnification on the right. ZrO_2 and glass (g) phases are labeled in the right hand micrographs. Note that only the ZSTS20 shows evidence of immiscible glass formation: g1 is silica rich while g2 contains Al and Mg impurities.

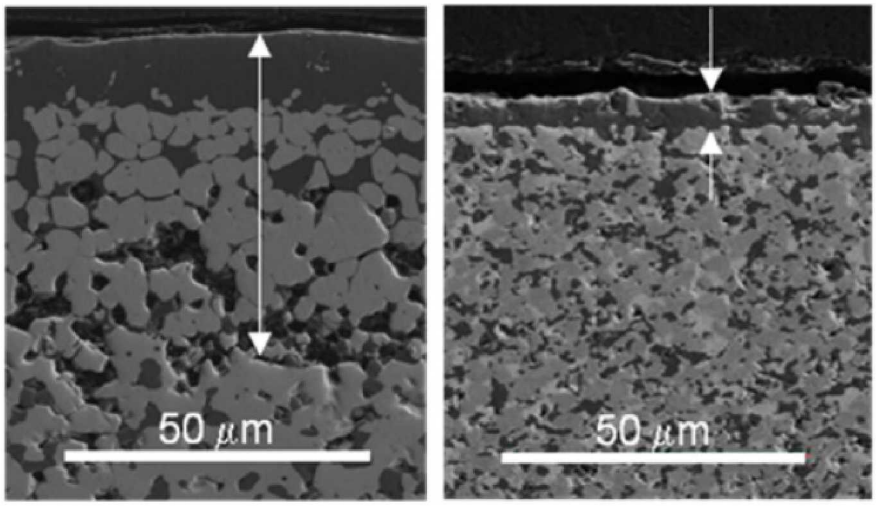

Fig. (4). Secondary electron images showing cross-sections of the ZS and ZSTS20 after oxidation at 1627°C for 100 min in stagnant air [10]. White arrows show the oxide thickness.

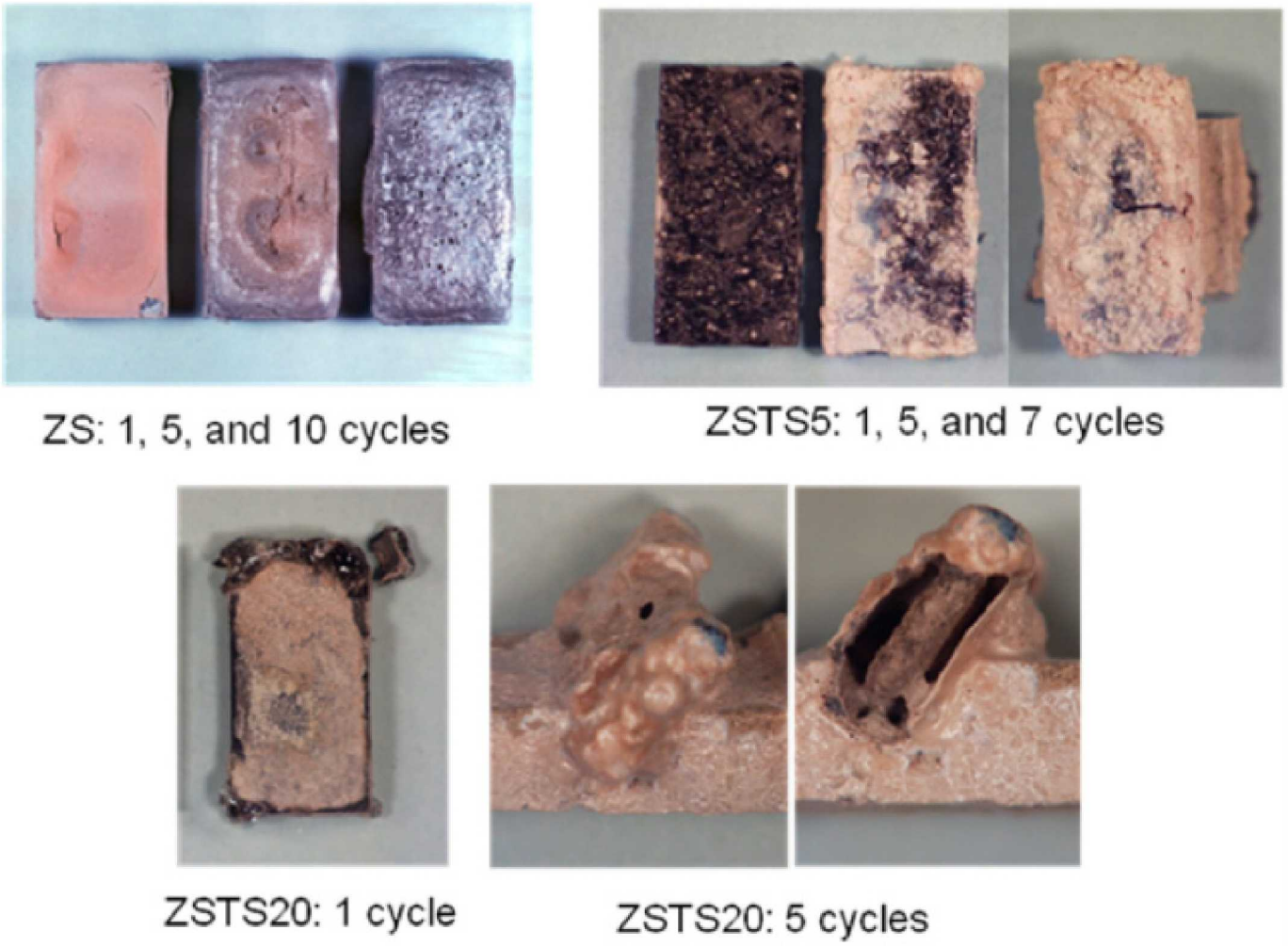

Fig. (5). Macrographs of ZS, ZSTS5, and ZSTS20 after oxidation at 1927°C for 10 minute cycles in stagnant air.

Table 3. Summary of Phases/Compositions Determined by WDS/Microprobe for ZSTS20 after Oxidation at 1927°C in Stagnant Air for 5 ten-Minute Cycles

Sample Location	ZrB_2	SiC	$TaSi_2$	$(Zr,Ta)B_x$	$(Zr,Ta)C_x$	ZrO_2 (at% Ta)	SiO_x (at% Ta)	$Ta(O,B)_x$	$Ta(C,B)_x$	$(Zr,Ta)O_x$
Substrate as hot-pressed	✓	✓	✓	✓ Zr/Ta=4.2 x=1.5						
Substrate after oxidation	✓	✓		✓ Zr/Ta= 3.5 x=1.4	✓ Zr/Ta=0.6 x=1.4					
Substrate near oxide interface	✓						✓ x=2.0			
Oxide near interface						✓ (0.2)	✓ x=2.0 (0.1)	✓ B/O=2.2 x=1.4		
Middle portion of attached scale						✓ (0.5)	✓ x=2.4 (1.6)	✓ B/O=1.7 x=0.7	✓ C/B=1.3 x=1.0	
Outer surface, detached scale						✓ (0.6, 1.3) 2 areas analyzed	✓ x=3.1 (2.5)			✓ Zr/Ta=1.9 x=2.5

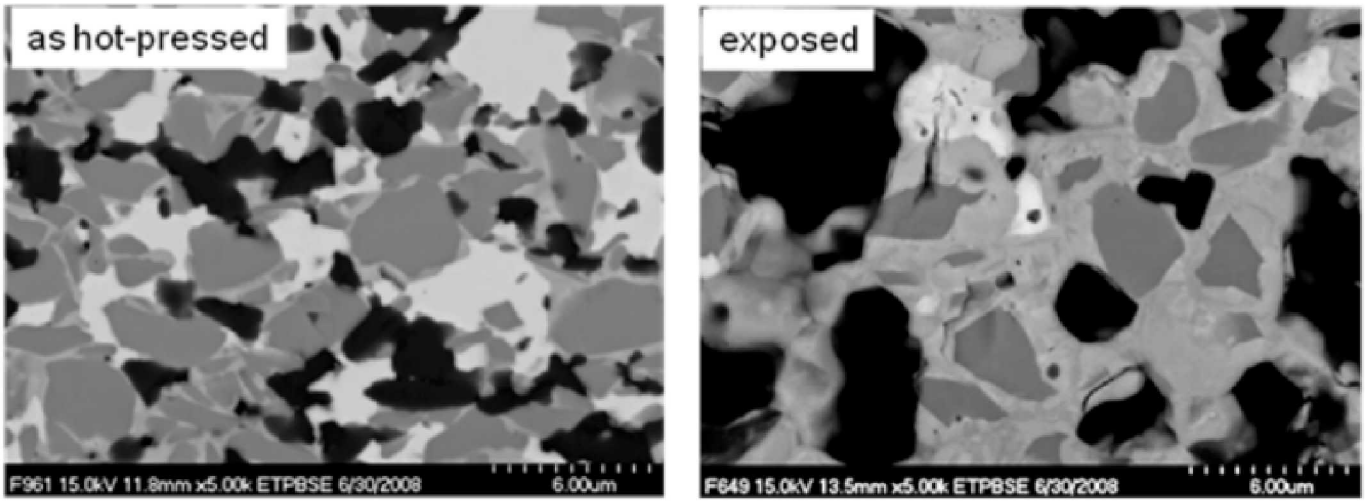

Fig. (6). Backscattered electron image of ZSTS20 substrate before and after oxidation for 50 min at 1927°C in stagnant air. Four phases are present in the hot-pressed material (from brightest to darkest contrast): $TaSi_2$, $(Zr,Ta)B_{1.5}$, ZrB_2, and SiC. The exposed sample contains (from brightest to darkest contrast) $(Zr,Ta)C_x$, $(Zr,Ta)B_x$, ZrB_2, SiC and porosity.

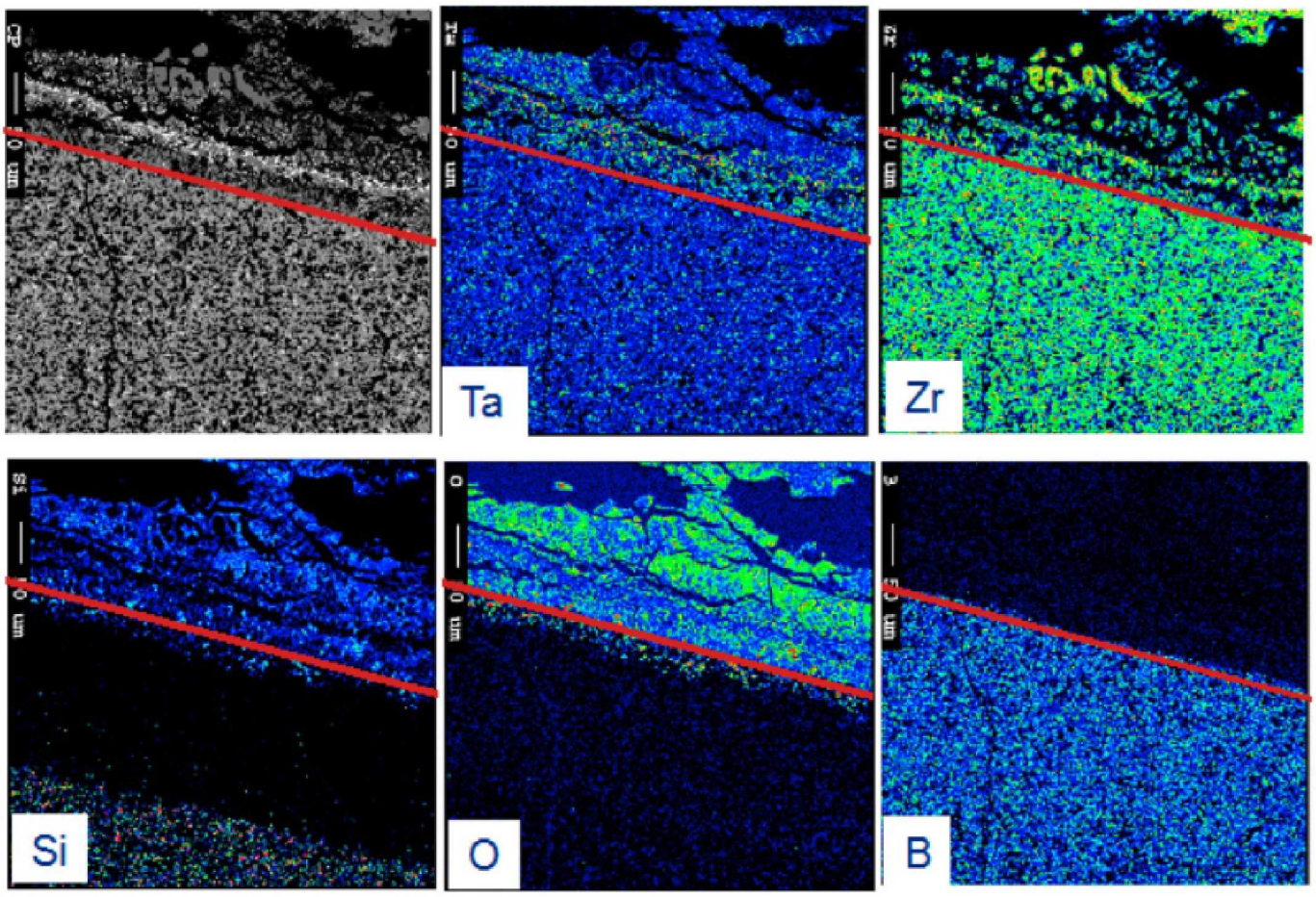

Fig. (7). Backscattered electron image and corresponding WDS dot maps for the substrate/oxide interface of ZSTS20 after oxidation at 1927°C for five 10-minute cycles in stagnant air. The red line corresponds to the approximate location of the ZrO_2/ZrB_2 interface as discussed in the text.

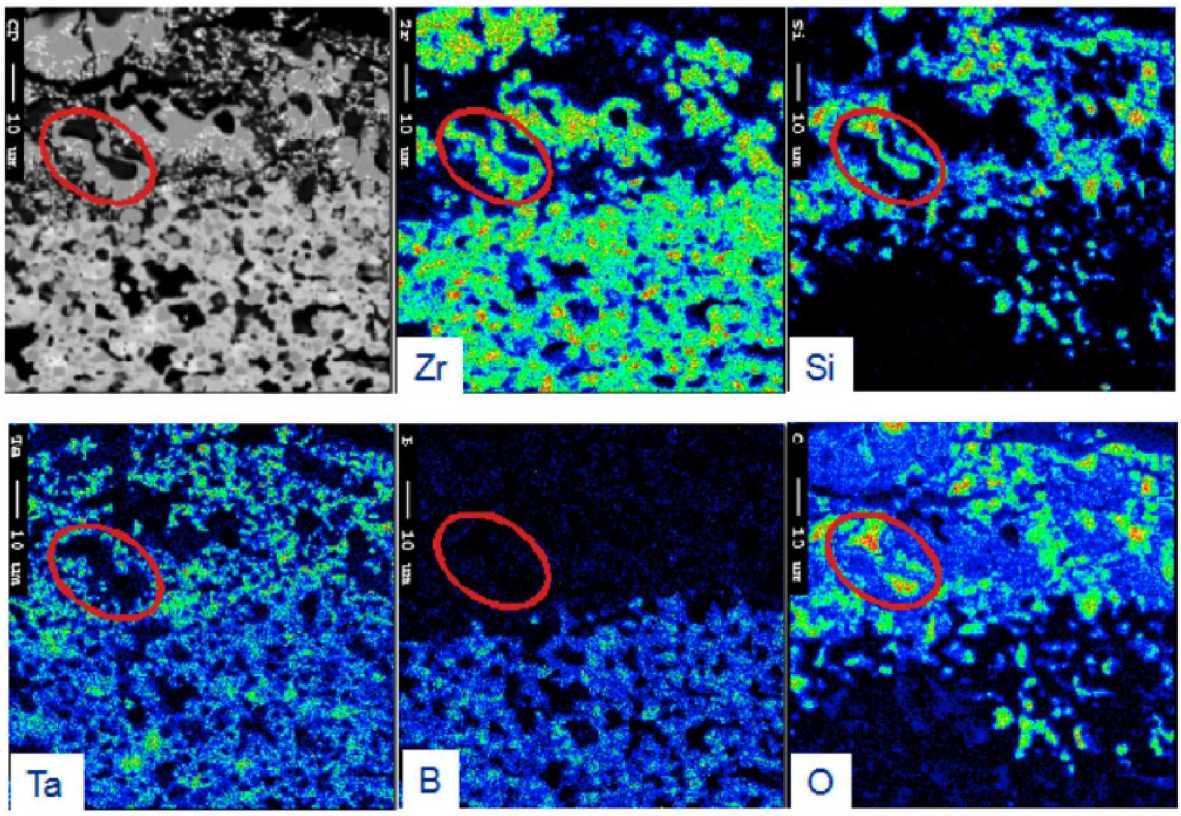

Fig. (8). Backscattered electron image and corresponding WDS dot maps for the substrate/oxide interface of ZSTS20 after oxidation at 1927°C for five 10-minute cycles in stagnant air. The red oval focuses on an area containing ZrO_2, SiO_2, and micron-sized, Ta-rich oxyboride phases.

Middle Portion of Attached Scale

The phases present in this portion of the scale are large columnar ZrO_2 grains in SiO_2, as shown in Fig. (**9**). In addition to the finely dispersed Ta oxyborides, a band of larger grains of Ta(C,B) is observed amongst the other oxide phases. Finally, the ZrO_2 grains appear to show surface reaction with the surrounding amorphous phase, as shown in Fig. (**10**).

Outer Surface, Detached Scale

The phases observed on the outer detached scale and shown in Fig. (**11**) include ZrO_2 found both as large grains and as dendrites, SiO_x with small amounts of dissolved Ta

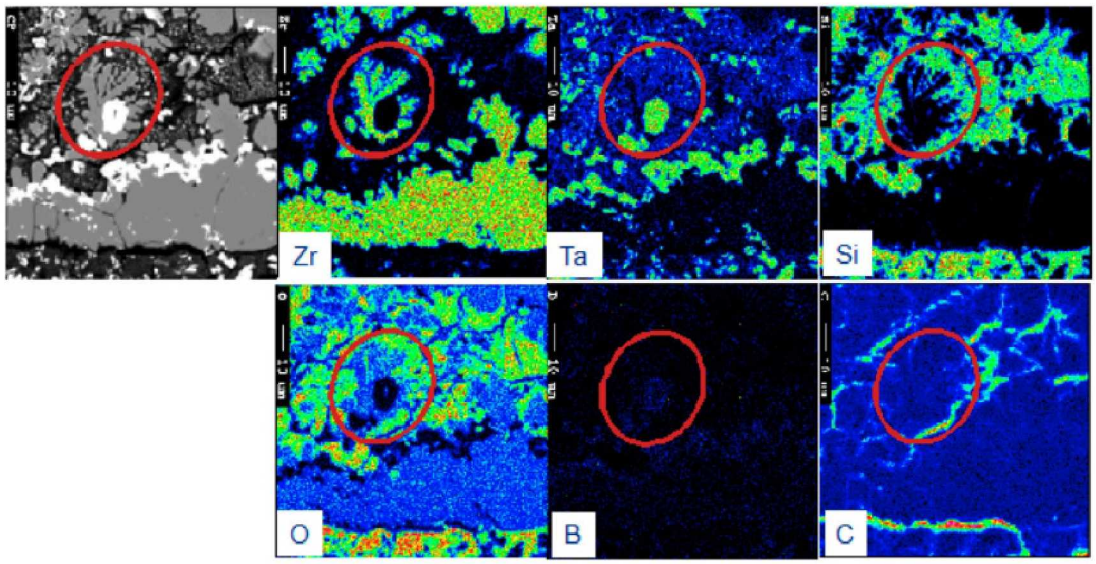

Fig. (9). Backscattered electron image and corresponding WDS dot maps for the middle of the oxide scale formed on ZSTS20 after oxidation at 1927°C for five 10-minute cycles in stagnant air. The red oval focuses on an area containing Ta(C,B) (brightest phase).

and Zr and x=3, and a (Zr,Ta) oxide with a cation/anion stoichiometry of 2:5 as would be expected for Ta_2O_5, however, two thirds of the cations are Zr.

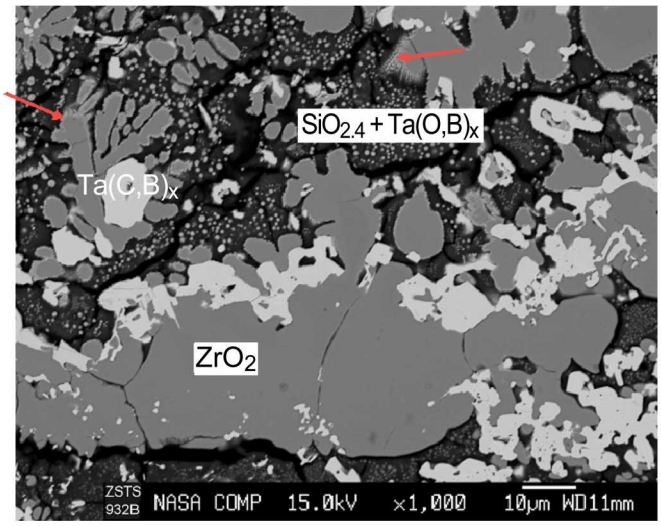

Fig. (10). Backscattered electron image of the middle of the oxide scale formed on ZSTS20 after oxidation at 1927°C for five 10-minute cycles in stagnant air. Same area as Fig. (**9**). The red arrows highlight the bright contrast surface layer found on zirconia suggesting Ta-enrichment.

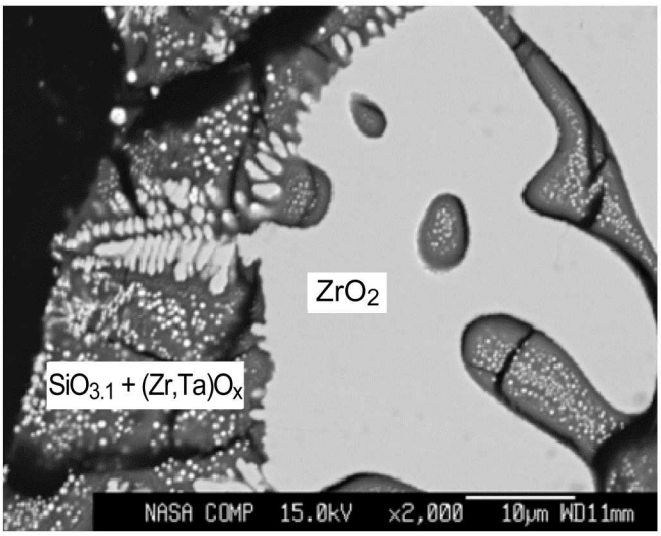

Fig. (11). Backscattered electron image of zirconia dendrites observed on the outer detached oxide scale formed on ZSTS20 after oxidation at 1927°C for five 10-minute cycles in stagnant air

DISCUSSION

Optimization of $TaSi_2$ Content

Twenty vol % addition of $TaSi_2$ to ZS promoted improved oxidation behavior at 1627°C. Both the weight change (Fig. **1**) and the oxide thickness (Fig. **4**) confirm this result. The appearance of the oxide surface indicates glass immiscibility, as shown in Fig. (**3**). Talmy *et al* [7-9] attribute similar observations of glass immiscibility to Ta additions to the system. EDS analysis [10] of the immiscible phases in Fig. (**3**) were inconclusive. The darkest phase showed EDS consistent with SiO_2. The medium contrast phase showed results consistent with Al and Mg impurities concentrated in a SiO_2-rich phase. In addition, a trace peak attributed to Ta and or Zr was also observed [10]. The bright phase had EDS results consistent with ZrO_2 and a slight trace of Ta or Si. The trace of Ta or Si could be oxide doping or a sampling volume effect. The sample was unavailable for further microprobe analysis to better characterize the composition of the surface oxide phases since it had been cross-sectioned, mounted and polished for oxide thickness measurements. Thus, while glass immiscibility has been observed, the mechanism for improved oxidation resistance due to Ta additions is still not certain.

The oxidation weight gain of ZSTS5 was similar to ZS (no $TaSi_2$ additions) at 1627°C. After only ten minutes of oxidation the ZSTS5 scale showed significant amounts of the pink scale observed previously for the ZSTS20 samples (Fig. **2**). However, this pink oxide was not able to establish a protective scale at longer times and the glassy appearance of the ZSTS5 after ten cycles was similar in appearance to the ZS material. SEM images of the surface oxide (Fig. **3**) show more uniform dispersion of the ZrO_2 in a continuous silica-rich phase relative to ZS, but glass immiscibility of the oxidized ZSTS20 was not observed.

At 1927°C, it was hoped that the reduction in $TaSi_2$ from 20 to 5 vol % would eliminate the excess liquid formation attributed to Ta-containing low melting phases, possibly by incorporation of the Ta into the ZrO_2. While five vol % $TaSi_2$ additions to ZS did reduce the amount of liquid phase relative to ZSTS20, there was still formation of significant amounts of liquid phase indicated by sample distortion, as shown in Fig. (**5**).

Not only did the reduction in $TaSi_2$ to 5 vol % fail to provide additional oxidation protection to ZS at 1627°C, the reduction was not enough to eliminate liquid phase formation at 1927°C. Thus, optimization of $TaSi_2$ content is not possible to allow improved oxidation behavior at both 1627 and 1927°C.

Characterization of ZSTS20 Before and After Oxidation at 1927°C in Stagnant Air for 50 Minutes

Substrate Phases: As Hot-Pressed

The composition of the hot-pressed material is summarized in Table **3** while images of the material can be seen in Fig. (**6**). The formation of $(Zr,Ta)B_{1.5}$ indicates that $TaSi_2$ is unstable with respect to ZrB_2. The stoichiometry of the new phase $(Zr,Ta)B_{1.5}$ suggests that Ta is added into the ZrB_2 structure without additional boron, resulting in a material with a lower relative boron content. XRD results indicated that the lattice parameters of the $(Zr,Ta)B_{1.5}$ phase were slightly smaller. These results are consistent with substitution of the smaller Ta atom on the Zr site and/or incorporation of B vacancies in the (Zr,Ta)-diboride phase. Table **4** shows the relative thermodynamic stability of a series of compounds important for this material system [5]. It can be seen that silicides are the least stable with Ta compounds less stable than the corresponding zirconium-based compounds. These trends are consistent with the

observed conversion of $TaSi_2$ to $(Zr,Ta)B_{1.5}$ during hot-pressing.

Table 4. Free Energy of Formation ΔG_f 1927°C(kJ/mol) $M+X_x=MX_x$ for Compounds of Interest in the ZSTS System [5]. Values for Ta_2O_5 are Shown Normalized for 1 Ta and 1 O_2 for Comparison to Other Phases

$TaSi_2$	-38	$ZrSi_2$	-121
TaC	-140	ZrC	-177
TaB_2	-189	ZrB_2	-277
$TaO_{2.5}$	-834	ZrO_2	-692
$Ta_{0.8}O_2$	-451		

Substrate Phases: After Oxidation at 1927°C

After oxidation, no $TaSi_2$ was observed in the matrix. In addition to ZrB_2, SiC, and $(Zr,Ta)B_{1.5}$, a new phase $(Ta,Zr)C_{1.4}$ is formed. The amount of the $(Zr,Ta)B_{1.4}$ has increased, the tantalum content in this boride phase has increased and the resulting B stoichiometry has also decreased slightly consistent with more Ta addition to the structure. This suggests continued reaction between $TaSi_2$ and ZrB_2. A possible explanation for additional loss of $TaSi_2$ and the appearance of both voids and the tantalum-rich carbide could be a reaction of the following form:

$$TaSi_2 + SiC + 1.5\ O_2(g) = TaC + SiO(g),\ \Delta G_{rxn} = -79kJ/mol \quad (1)$$

with the free energy data obtained from the FACT database [5]. This reaction is a type of active oxidation in which both $TaSi_2$ and SiC are consumed forming TaC as the silicon leaves the system as a vapor species. TaC is more stable than SiC (ΔG_f 1927°C= -140kJ/mol *vs* -41kJ/mol) [5] making this a likely reaction route.

Oxide Phases Formed: ZrO_2

ZrO_2 is observed as large grains tending toward a columnar structure throughout the scale. The amount of Ta dissolved in the ZrO_2 structure increased toward the outer surface of the oxide, but remained low, 1.3 at% or less. This suggests that incorporation of Ta into the ZrO_2 is limited for *in situ* thermally grown oxides. Higher contents of Ta_2O_5 have been incorporated in zirconia by traditional powder or sol gel ceramic processing techniques [18-20]. There are two consequences of this limited solubility of Ta in thermally grown zirconia. First, oxygen ion transport through the zirconia will not be reduced substantially due to oxygen vacancy concentration reduction associated with pentavalent Ta occupying quadravalent zirconium sites. Ionic conductivity and ion diffusivities are related through the Nernst Einstein equation [21]. Thus, oxygen ionic conductivity measurements as a function of dopant concentration can give information about the changes in oxygen diffusivity. While data for the dependence of ionic conductivity in Ta_2O_5-doped ZrO_2 are not available in the literature, data obtained for ZrO_2 co-doped with Y_2O_3 and Ta_2O_5 show less than an order of magnitude decrease in ionic conductivity for 2mol% Ta_2O_5 additions [22,23]. Thus, a Ta_2O_5 content of about 1% in ZrO_2 is not likely to substantially reduce the oxidation rates of ZS materials. Second, since solubility of Ta in thermally grown ZrO_2 is limited, any excess Ta is likely to form low melting oxide phases which are detrimental to oxidation resistance at temperatures exceeding their melting point. The formation of zirconia dendrites shown in Fig. (**11**) is evidence of zirconia incorporation in and precipitation from these low melting phases.

There is additional evidence of zirconia reaction with Ta in the bright contrasting phases formed around each zirconia grain as seen in Fig. (**10**). Microprobe was not conducted on these surface reaction phases, so the composition is unknown. One possibility is that this phase is the V-phase, Ta_2O_5-xZrO_2 (x = 5 to 8). An additional zirconium tantalate phase was observed phase separated in the silica in the outer detached layer of the oxide scale, though this phase has the 2:5 stoichiometry of Ta_2O_5.

Oxide Phases Formed: SiO_2

SiO_2 is observed as the continuous phase that surrounds the columnar zirconia grains as well as any Ta-containing phases. Microprobe results indicate the expected SiO_2 oxygen stoichiometry near the oxide/substrate interface. The oxygen stoichiometry deviates moving outward through the oxide scale while correspondingly more Ta is incorporated in the silica. A maximum of 2.5 at% Ta is observed in the silica. At the outer surface, small spheroids of phase-separated zirconium tantalate are observed in the silica as previously mentioned and shown in Fig. (**11**). The stoichiometric and compositional trends indicate that "pure" silica is formed at the oxide/matrix interface and more complex silicate melts are formed in the outer portion of the oxide as the scale thickens.

Oxide Phases Formed: Ta-Oxides

Ta_2O_5, the thermodynamically stable oxide of Ta is not observed anywhere in the oxide scale. Near the substrate/oxide interface, small submicron precipitates of Ta-oxyboride are dispersed in both the ZrO_2 and the SiO_2 (Fig. **8**). The observation that these particles are dispersed in the zirconia supports the limited solubility of Ta in the ZrO_2.

Proceeding outward through the scale, larger 10 μm sized particles of Ta(C,B) grains are observed in a layered structure (bright phase in Fig. **9**). This layer corresponds to the highest concentration of Ta observed in the oxide scale as shown in Fig. (**7**). The existence of these large non-oxide grains is surprising since they are surrounded by oxide. However, based on the Ellingham diagram calculated using the Fact database [5] shown in Fig. (**12**), tantalum oxides are the least thermodynamically stable, so that for a limited amount of oxygen, zirconia is expected to form preferentially. A similar phenomenon was observed in which BN remained unoxidized when surrounded by SiO_2 due to the relative thermodynamic stabilities of the boria and silica [24].

As discussed above, two zirconium tantalate phases are observed in the outer portions of the scale while more Ta is observed dissolved in both the zirconia and the silica. These

more complex tantalates are found in the outer portions of the scale suggesting further Ta reactions occur at longer exposure times.

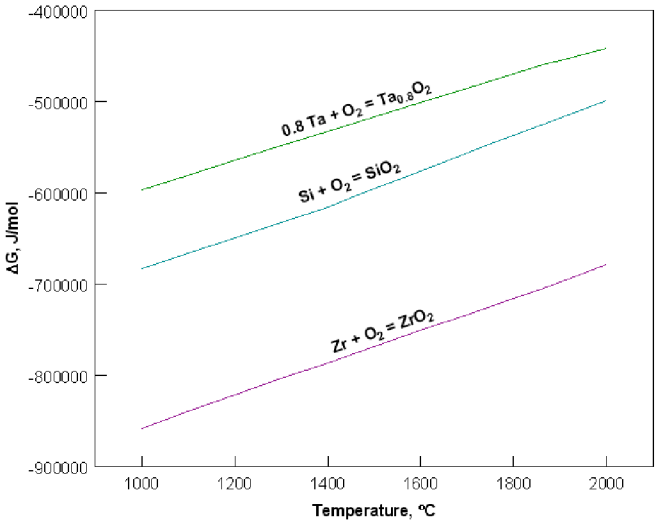

Fig. (12). Ellingham diagram for oxides in the ZSTS system calculated with FACT53 data and FactSage [5].

CONCLUSIONS

Previous results [10] have shown that additions of 20 v% $TaSi_2$ to ZrB_2-20 v% SiC resulted in markedly improved oxidation resistance at 1627°C in air for 100 minutes. This improved oxidation resistance is likely attributed to Ta-induced glass phase immiscibility and resulting lower transport rates of oxygen through the more viscous glasses. However, it has now been demonstrated that addition of the smaller amount of 5 v% $TaSi_2$ to ZrB_2-20 v% SiC is insufficient to result in glass immiscibility and improved oxidation resistance. $TaSi_2$ additions to ZrB_2-20 v% SiC in both 5 and 20 v% amounts resulted in extensive liquid phase formation when exposed for 50 minutes in stagnant air at 1927°C. Extensive microprobe characterization of the 20 v% $TaSi_2$-containing sample, 1927°C exposure, has shown that $TaSi_2$ additions are not suitable for applications at 1927°C for a number of reasons. $TaSi_2$ is unstable in the matrix with respect to ZrB_2. During oxidation, $TaSi_2$ in the presence of SiC appears to undergo active oxidation forming TaC and SiO(g) leaving voids in the substrate. During oxidation, Ta is incorporated in the zirconia in amounts of 1.3 at% or less, suggesting that in-situ doping of the zirconia to decrease oxygen transport rates through the zirconia is limited. During oxidation, Ta also forms oxyboride, silicate, and zirconate phases which result in extensive amounts of liquid phase formation and poor oxidation resistance. Ta-additions to ZrB_2-20 v% SiC are not recommended for ultra-high temperature (>1900°C) applications.

ACKNOWLEDGEMENTS

The authors would like to acknowledge Ralph Garlick (GRC, deceased) for the x-ray diffraction results and Jim Nesbitt (GRC) for a careful review of this paper. This work was funded by NASA Next Generation Launch Technology Program, Airframe Technology Project and the NASA Fundamental Aeronautics Program, Hypersonics Project.

REFERENCES

[1] W.G. Fahrenholtz, G.E. Hilmas, I.G. Talmy, and J.A. Zaykoski, "Refractory diborides of zirconium and hafnium," *J. Am. Ceram. Soc.*, vol. 90, pp. 1347-1364, May 2007.

[2] J.B. Berkowitz-Mattuck, "High temperature oxidation III. Zirconium and hafnium diborides," *J. Electrochem. Soc.*, vol. 113, pp. 908-914, Sep 1966.

[3] E.V. Clougherty, R.L. Pober, and L. Kaufman, "Synthesis of oxidation resistant metal diboride composites," *Trans. Metall. Soc.*, vol. 242, pp. 1077-1082, June 1968.

[4] X.-H. Zhang, P. Hu, and J.-C. Han, "Structure evolution of ZrB_2-SiC during the oxidation in air," *J. Mater. Res.*, vol. 23, pp. 1961-1972, July 2008.

[5] C.W. Bale, P. Chartrand, S.A. Decterov, G. Eriksson, K. Hack, R. Ben Mahfoud, J. Melançon, A.D. Pelton, and S. Petersen, "FactSage thermochemical software and databases", *Calphad J.*, vol. 62, pp. 189-228, 2002.

[6] X. Zhang, P. Hu, J. Hun, and S. Meng, "Ablation behavior of ZrB_2-SiC ultra high temperature ceramics under simulated atmospheric re-entry conditions," *Comp. Sci. Technol.*, vol. 68, pp. 1718-1726, 2008.

[7] I.G. Talmy, J.A. Zaykoski, M.M. Opeka, and S. Dallek, "Oxidation of ZrB_2 ceramics modified with SiC and group IV-VI transition metal diborides," in *High Temperature Corrosion and Materials Chemistry III,* Electrochemical Society Proceedings Volume 2001-12, M. McNallan, and E. Opila, Eds., Pennington, NJ: The Electrochemical Society, Inc., 2001, pp. 144-158.

[8] I.G. Talmy, J.A. Zaykoski, M.M. Opeka, and A.H. Smith, "Properties of ceramics in the system ZrB_2-Ta_5Si_3," *J. Mater. Res.*, vol. 21, pp. 2593-2599, Oct. 2006.

[9] I.G. Talmy, J.A. Zaykoski, and M.M. Opeka, "High-temperature chemistry and oxidation of ZrB_2 ceramics containing SiC, Si_3N_4, Ta_5Si_3, and $TaSi_2$," *J. Am. Ceram. Soc.*, vol. 91, pp. 2250-2257, July 2008.

[10] E. Opila, S. Levine, and J. Lorincz, "Oxidation of ZrB_2- and HfB_2-based ultra-high temperature ceramics: effect of Ta additions", *J. Mater. Sci.*, vol. 39, pp. 5969-5977, 2004.

[11] HSC http://www.outotec.com/pages/Page____35369.aspx?epslanguage=EN (Feb, 20, 2010).

[12] T. Ya. Kosolopova, *Handbook of High Temperature Compounds: Properties, Production, Applications*. NY: Hemisphere Publishing Corp, 1990, pp. 162.

[13] A. Reisman, F. Holtzberg, M. Berkinblit, and M. Berry, "Reactions of the group VB pentoxides with alkali oxides and carbonates III. Thermal and X-Ray phase diagrams of the system K_2O or K_2CO_3 with Ta_2O_5," *J. Am. Chem. Soc.*, vol. 78, pp. 4514-4520, Sep. 1956.

[14] B.W. King, J. Schultz, E.A. Durbin, and W.H. Duckworth, "Some properties of tantala systems," Battelle Memorial Institute Report No. BMI-1106, 1956.

[15] Powder Diffraction File, International Centre for Diffraction Data, Swarthmore, Pennsylvania, card no. 42-60.

[16] H.M. Ondik, and H.F. McMurdie, Eds. *Phase Diagrams For Zirconium And Zirconia Systems*, Westerville, OH: The American Ceramic Society, 1998, p. 144.

[17] S.R. Levine, and E.J. Opila, "Tantalum addition to zirconium diboride for improved oxidation resistance," NASA-TM 2003–212483, 2003.

[18] M.M. Abou Sekkina, M.A. Ewaida, E.M. Ibrahim, and A.A. Al-Awady, "Investigations of microstructural changes and spectral characteristics of tantala stabilized zirconia refractories," *Polym. Degrad. Stab.*, vol. 19, pp. 273-278, 1987.

[19] M.A. Ewaida, M.M. Abou Sekkina, E.M. Ebrahim, and A.A. Al-Adawy, "Novel studies on the thermoelectro-mechanical properties of tantala-doped zirconia refractories," *Polym. Degrad. Stab.,* vol. 21, pp. 227-235, 1988.

[20] G. Gritzner, C. Puchner, A. Pissenberger, and J. Dusza, "Vanadia, niobia, and tantala doped zirconia," in *Ceramics, Charting the Future*, p. Vincenzini, Ed. Faenza – Italy: Techna Srl, 1995, pp. 1411-1417.

[21] P. Kofstad, *Nonstoichiometry, Diffusion, and Electrical Conductivity in Binary Metal Oxides*, Wiley-Interscience, New York, 1972.

[22] M. Caillet, C. Deportes, G. Robert, G. Vallier, and G. Vitter, "Structure et conductivite electrique a haute temperature dans le systeme ZrO_2-Y_2O_3-Ta_2O_5," *Rev. Int. Hautes. Temper. et Refract.*, vol. 5, pp. 173-179, 1968.

[23] A.G. Kotlyar, A.D. Neuimin, S.F. Pal'guev, V.N. Strekalovskii, and V.N. Zubankov, "Structure and electrical conductivity in the system ZrO_2-Y_2O_3-Ta_2O_5," *Inorg. Mater.*, vol. 6, pp. 281-285, Feb 1970.

[24] B.W. Sheldon, E.Y. Sun, S.R. Nutt, and J.J. Brennan, "Oxidation of BN-coated SiC fibers in ceramic matrix composites," *J. Am. Ceram. Soc.,* vol. 79, pp. 539-43, Feb 1996.

Received: September 8, 2009 Revised: December 21, 2009 Accepted: December 23, 2009